IEICE TRANSACTIONS

on Electronics

DOI:10.1587/transele.2023ECP5059

Publicized:2024/08/15

A PUBLICATION OF THE ELECTRONICS SOCIETY

The Institute of Electronics, Information and Communication Engineers
Kikai-Shinko-Kaikan Bldg., 5-8, Shibakoen 3chome, Minato-ku, TOKYO, 105-0011 JAPAN

PAPER

Design Procedures of Decoupling Circuit Utilizing Coupling Between Antennas

Zhi Earn TAN[†], ***Student Member***, **Kenjiro MATSUMOTO**[†], **Masaya TAKAGI**[†], **Hiromasa SAEKI**[††], ***Nonmembers***, ***and*** **Masaya TAMURA**[†], ***Senior Member***

SUMMARY This paper presents novel design procedures for a decoupling circuit, utilizing the coupling between antennas. The proposed decoupling circuit consists of, a Band-Stop Filter (BSF) based on Coupling Matrix Synthesis(CMS) theory, a pair of matching circuits, and microstrip connecting lines. By inserting a BSF into an antenna pair, high isolation can be achieved. By utilizing coupling between antennas, the proposed BSF can be designed only using 2 parallel resonators based on the CMS theory. To maintain impedance matching of patch antennas, a pair of matching circuits is inserted after the BSF for each port. Lastly, the decoupling circuit model was fabricated. The experimental results have a good agreement with the simulation result and the validity of the proposed design method is confirmed.

key words: *Decoupling-Matching Network, In-Band Full-Dulpex(IBFD), Self-Interference Cancellation (SIC), Multiple-Input-Multiple-Output (MIMO), Band-Stop Filter (BSF), Coupling Matrix Synthesis (CMS)*

1. Introduction

In recent years, the number of IoT (Internet of Things) devices has been increasing drastically year by year, Multiple-Input-Multiple-Output (MIMO) [1] and In-Band Full-Duplex (IBFD) [2] technologies have attracted tremendous attention as methods of realizing high-capacity communication to overcome the problem of exhaustion of available frequency spectrum. However, in applications requiring compact layouts, the electromagnetic coupling formed between adjacent antennas causes various problems. For example, the radiation efficiency, signal-to-noise ratio, and channel capacity are degraded due to channel correlation in MIMO applications [3][4]. While in IBFD, the degradation of the signal-to-noise ratio due to self-interference causes problems that make communication become impossible [5][6]. Therefore, various decoupling techniques have been proposed to remove the coupling between antennas.

One of the simplest methods is suppression of coupling by the orthogonal arrangement of antennas [7]–[15]. While this method can achieve high isolation, but it makes the antenna layout more difficult and requires a large implementation space. The suppression of the coupling between antennas can be also realized by using decoupling network [16]–[21]. In [18]–[21], decoupling is achieved by connecting the coupling path through a resonator in parallel with the coupling between antennas. In [18]–[19], wideband decoupling is achieved by designing a coupling path through a second-order resonator.

However, the design method for multi-stage resonators is not clarified in these papers. Broader frequency coverage and better suppression of mutual coupling across a wider frequency range can be achieved by utilizing multiple resonant stages compared to single-stage resonators. This improvement is attributed to the increased degree of freedom in the design of the band-stop filter. In this paper, a novel method and steps for designing a decoupling network using BSF based on CMS filter theory with a 2-order parallel resonator topology are presented. This allows the design of a decoupling circuit with the desired number of resonator stages. For the purpose of saving mounting space, a parallel-coupled BSF with resonators coupled in parallel is adopted, while the direct source/load (S/L) coupling is replaced by the coupling between the antennas. In addition, the characteristics of Y_{21}, which are important in BSF designed CMS filter theory, are verified to confirm that the designed circuit works as a BSF. Given the crucial role of the Q factor in influencing the performance of the band-stop filter, it is imperative to thoroughly explore methods for preserving this parameter within the filter's elements. As such, forthcoming chapters will delve into a comprehensive discussion on strategies and techniques aimed at maintaining the Q factor. As a design example, two monopole antennas operating in the 840-MHz band with a 10 MHz bandwidth, suitable for cellular communication systems, are used, and a decoupling network is designed by using chip elements and short-stub resonators. These antennas leverage the frequencies within the United States' Cellular Band (824-894 MHz), which encompasses 840 MHz.

2. Principle of Proposed Decoupling Circuit

2.1 Proposed Decoupling Netwrok Structure

In this study, a BSF-based decoupling circuit is inserted in parallel between the antennas to cancel off self-interference signals caused by the coupling between the antennas as shown in Fig.1. According to reference [4], for the realization of IBFD, self-interference cancellation of 50 dB or more is required in the analog stage. However, in this study, priority is given to the establishment of a design methodology, and therefore, the isolation target value is set to a feasible

[†]Department of Electrical and Electronic Information Engineering, Toyohashi University of Technology, Toyohashi-shi, 441–8580 Japan.

[††]Murata Manufactureing Co., Ltd.

30 dB achievable with a simple structure. In this section, the theory and the design flow of the proposed decoupling circuit are described.

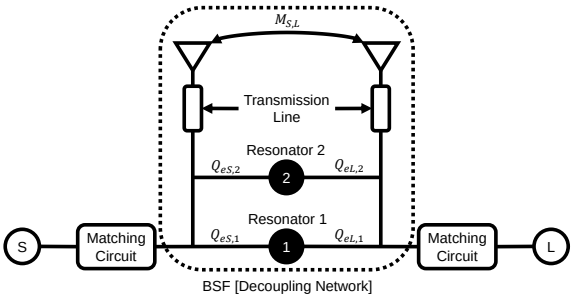

Fig. 1 Decoupling Circuit Utilizing Coupling between Antennas.

When designing the proposed decoupling circuit, the following three design conditions must be fulfilled for realising the desired decoupling circuit. Here, the values listed in the conditions are the desired values required to achieve an isolation of 30 dB between antennas. Note that these values are crucial for optimal performance.

- Suppressing the real part of the transmission admittance $\mathrm{Re}[\mathrm{Y}_{21}]$ between antennas in the range ±0.001 within the target decoupling bandwidth.
- Suppressing the imaginary part of the transmission admittance $\mathrm{Im}[\mathrm{Y}_{21}]$ between antennas in the range ±0.001 within the target decoupling bandwidth.
- Ensuring the return loss at the center frequency is less than -10 dB.

To satisfy the conditions mentioned above, three main components are required, as shown in Fig.1 : a transmission line connecting the antennas to the BSF, the BSF itself, and the matching circuits. Hence, the design of the proposed decoupling circuit can be undertaken as follows.

1. Design of Antenna
    - Conduct electromagnetic simulation using High-Frequency Simulation Software (HFSS, Ansys) for antenna design.
2. Optimization of Transmission Line Length
    - Suppress $\mathrm{Re}[\mathrm{Y}_{21}]$ between antennas by optimizing the transmission line length.
    - Utilize the transmission line as a phase shifter.
    - Determine the width of the transmission line for impedance matching (50 Ω).
3. Deviation of Coupling Coefficient of Antennas
    - Derive the coupling coefficient before starting the BSF design.
    - The reason for this is that the BSF is primarily employed to suppress $\mathrm{Im}[\mathrm{Y}_{21}]$ rather than $\mathrm{Re}[\mathrm{Y}_{21}]$.
4. Design of BSF
    - Calculate the coupling matrix based on derived coupling coefficient.
    - Design the BSF utilizing the coupling between antennas with the circuit simulator (PathWave Advanced Design System, ADS) based on the calculated coupling matrix.
5. Design of Decoupling Circuit
    - Insert the designed BSF between the antennas in parallel to suppress $\mathrm{Im}[\mathrm{Y}_{21}]$.
6. Design of Matching Circuit
    - Design a matching circuit to address antenna impedance mismatch due to the insertion of BSF.
7. Fabrication and Evaluation
    - Evaluate S-parameters, transmission admittance, and directivity.

2.2 Design Theory of BSF

In this section, we will discuss the design procedures of a BSF based on the Coupling Matrix Synthesis theory [22][23] as shown in Fig.2. Before initiating the BSF design, it is essential to consider the coupling coefficient of the antenna in the characteristic parameters of the BSF. In particular, eliminating the direct S/L coupling component of the BSF through the utilization of coupling between antennas is crucial for our proposed method.

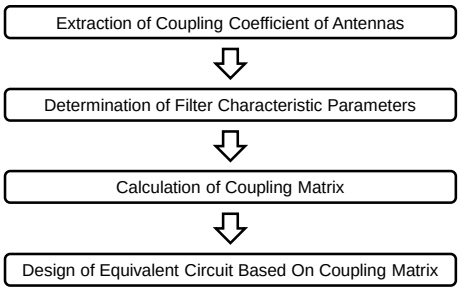

Fig. 2 Design Procedure Flow Chart of BSF.

2.2.1 Coupling Matrix

The coupling matrix is calculated using the method presented in references [22]–[26]. Here, the example of the coupling matrix of 4×4 is given in Eq.(1). Eq.(1) represents the calculated coupling matrix based on the topology as shown in Fig.1. The definitions of each matrix component are also summarized below. Usually, the coupling matrix of a common band-pass filter (BPF) does not contain a direct S/L coupling component which is $M_{S,L}$ showing in Eq.(1). However, the direct S/L coupling component is required for BSF to invert the S_{11} and S_{21} to generate band-stop characteristics.

$$M = \left(\begin{array}{c|cccc} & S & 1 & 2 & L \\ \hline S & 0 & \pm M_{S,1} & \pm M_{S,2} & \pm M_{S,L} \\ 1 & \pm M_{S,1} & \pm M_{1,1} & 0 & \pm M_{1,L} \\ 2 & \pm M_{S,2} & 0 & \pm M_{2,2} & \pm M_{2,L} \\ L & \pm M_{S,L} & \pm M_{1,L} & \pm M_{2,L} & 0 \end{array} \right) \quad (1)$$

where,

- $M_{i,i}(i = 1, 2)$:the self-coupling coefficient of the i-th resonator.
- $M_{S,i}$ or $M_{L,i}(i = 1, 2)$:The coupling coefficient between the source or load and the i-th resonator.
- $M_{S,L}$:The direct S/L coupling coefficient.

The coupling matrix components of each row contain either a positive or negative sign, indicating whether the resonant mode of each resonant path is an even mode or an odd mode. The relationship between the sign of the coupling coefficient and the resonant mode is shown in Eq.(2) [26].

$$M_{S,i} = \left\{ \begin{array}{ll} +M_{i,L} & \text{for even mode} \\ -M_{i,L} & \text{for odd mode} \end{array} \right\} \quad (2)$$

To design the equivalent circuit of the BSF, it is necessary to convert the values of the coupling matrix components into the indices commonly used in filter design. The diagonal component of the coupling matrix can be converted into the resonant frequency using Eq.(3) [26], while the coupling coefficient between the source and the resonator, as well as between the load and the resonator, can be converted to the external Q of the resonator using Eqs.(4) and (5) [26].

$$f_i = \frac{-BW \cdot M_{i,i} + \sqrt{BW^2 \cdot M_{i,i}^2 + 4f_0^2}}{2} : i = 1, 2 \quad (3)$$

$$\text{Source side} \ : \ Q_{eS,i} = \frac{f_i}{BW \cdot M_{S,i}^2} \quad (4)$$

$$\text{Load side} \ : \ Q_{eL,i} = \frac{f_i}{BW \cdot M_{L,i}^2} \quad (5)$$

As the external Q-factor of the resonator is influenced by both the source and load sides simultaneously, the actual value of Q_e can be obtained by Eq.(6).

$$Q_{e,i} = \frac{Q_{eS,i} Q_{eL,i}}{Q_{eS,i} + Q_{eL,i}} \quad (6)$$

2.2.2 Equivalent Circuit of BSF

The discussion focuses on the method for the conversion of an equivalent circuit for BSF in this section. The topology of BSF shown in Fig.1 is an example of the coupling matrix with signs based on the Eq.(7). The distinction in resonant modes can be illustrated by inserting J-inverters between the resonator, source, and load. Both J-inverters and resonators can be realized using simple inductor (L) and capacitor (C) components. Therefore, the equivalent circuit, as depicted in Fig.3, is constructed with the first resonant mode being odd and the second resonant mode being even, based on the topology shown in Fig.1.

$$\left(\begin{array}{cccc} 0 & -M_{S,1} & M_{S,2} & M_{S,L} \\ -M_{S,1} & -M_{1,1} & 0 & M_{L,1} \\ M_{S,2} & 0 & M_{2,2} & M_{L,2} \\ M_{S,L} & M_{L,1} & M_{L,2} & 0 \end{array} \right) \quad (7)$$

In this equivalent circuit, two attenuation poles emerge from

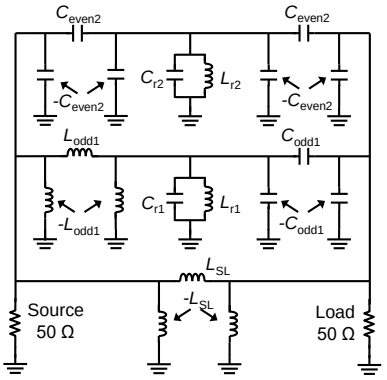

Fig. 3 Equivalent Circuit with Reactance Elements.

the phase differences in both even-mode and odd-mode coupling paths, as well as the phase difference between the even-mode coupling path and direct S/L coupling. Once the equivalent circuit of the BSF has been represented, the derivation of the element values in the circuit needs to be undertaken. The resonator's element values are constrained by the resonant frequency, but there is an infinite number of L and C combinations based on their ratio. These combinations share the same resonant frequency but impact the external Q. Since the external Q can be manipulated by an inverter, the determination of the resonator's L and C ratio is prioritized, enabling the straightforward determination of the inverter's value. Element values satisfying design indices are determined by iteratively adjusting the resonator and inverter values, as well as the values of the direct S/L coupling.

The resonant frequency $f_i^{'}$ of the resonant path can be also derived by Eq.(8) [27].

$$\left| \frac{d^2\phi}{df^2} \right|_{f=f_i^{'}} = 0 \quad (8)$$

Here, the reflection phase ϕ due to the resonator depends on each resonant mode of the resonator and can be obtained by Eqs.(9) and (10) [27].

$$e^{j\phi_{re}} = S_{11e} = S_{11} + S_{21} : \text{even mode} \quad (9)$$

$$e^{j\phi_{ro}} = S_{11o} = S_{11} - S_{21} : \text{odd mode} \quad (10)$$

At the resonant frequencies of each resonant mode, the resonators will be short-circuited and the reflection phases for

each resonant mode can be obtained using Eq.(11).

$$\phi_{ri}(\omega_{0i}) = n\pi; (n = \pm1, \pm3, \cdots) : i = \text{even , odd} \quad (11)$$

The external Q (Q'_{ei}) of the each resonant mode can be obtained by Eq.(12) [27].

$$Q'_{ei} = \frac{\omega}{2}\left|\frac{d\phi}{d\omega}\right|_{\omega=2\pi f_i} \quad (12)$$

To facilitate the visualization and easy attainment of design indices, the Eqs.(8)(9)(10)(12) below are derived as reference parameters, which can be observed through ADS. The determination of element values for the equivalent circuit can be easily accomplished based on these reference parameters with the assistance of ADS software.

One of the aims of this study is to eliminate the direct S/L coupling of the BSF by utilizing coupling between antennas. In the proposed decoupling circuit configuration, the antennas and the BSF are arranged in parallel. Therefore, by using the properties of the admittance (Y)-parameters and the coupling matrix derived from CMS theory, Eq.(13) can be obtained.

$$\begin{pmatrix} 0 & M_{S,1} & M_{S,2} & M_{S,L} \\ M_{S,1} & M_{1,1} & 0 & M_{L,1} \\ M_{S,2} & 0 & M_{2,2} & M_{L,2} \\ M_{S,L} & M_{L,1} & M_{L,2} & 0 \end{pmatrix} = \begin{pmatrix} 0 & M_{S,1} & M_{S,2} & 0 \\ M_{S,1} & M_{1,1} & 0 & M_{L,1} \\ M_{S,2} & 0 & M_{2,2} & M_{L,2} \\ 0 & M_{L,1} & M_{L,2} & 0 \end{pmatrix} + \begin{pmatrix} 0 & 0 & 0 & k \\ 0 & 0 & 0 & 0 \\ 0 & 0 & 0 & 0 \\ k & 0 & 0 & 0 \end{pmatrix} \quad (13)$$

where k is the coupling coefficient between antennas.

The left-hand side of Eq.(13) represents the coupling matrix of the BSF derived from CMS. Since the antennas and BSF are connected in parallel, the left-hand side of Eq.(13) can be decomposed into two matrices using the admittance parameter property. The second term on the right-hand side represents the coupling matrix between the antennas, while the first term represents the coupling matrix of the BSF which the direct S/L coupling is eliminated. Therefore, the direct S/L coupling $M_{S,L}$ can be nullified by the relation of $M_{S,L} = k$ in Eq.(13).

Note that eliminating the direct S/L requires deriving the coupling coefficient between the antennas. The coupling coefficient k between the antennas can be derived using Eq.(14). It's important to note that the sign of k cannot be determined because the derived k can only be positive as it represents the absolute value of the transmission S-parameter $|S_{21}|$ used in Eq.(14).

$$k = \pm\frac{1 - \sqrt{1 - |S_{21}|^2}}{|S_{21}|} \quad (14)$$

In this study, it is assumed that the sign of k varies with the type of coupling between antennas at the desired operating frequency. When the coupling between the antennas is inductive, the sign of k is positive while it is negative when the coupling between the antennas is capacitive. This assumption can be validated by constructing an equivalent circuit that represents the coupling between antennas with reference to the imaginary part of the transmission admittance $\mathrm{Im}[\mathrm{Y}_{21}]$ at the desired operating frequency as shown in Fig.4.

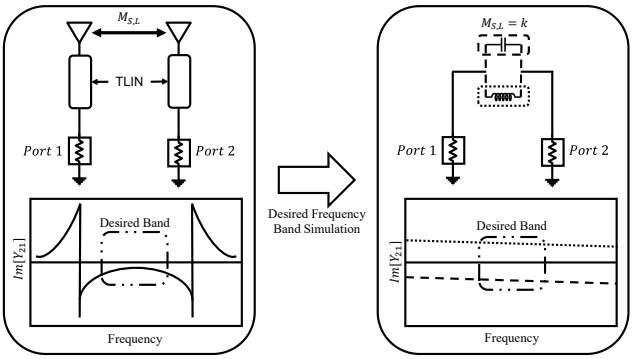

Fig. 4 Simulation Configuration of Coupling Coefficient.

As the transmission admittance between the antennas exhibits a non-linear characteristic, the equivalent circuit representing the coupling characteristics between the antennas is designed, considering only the desired bandwidth, as shown in Fig.4. Therefore, the tangent of the transmission admittance within the desired band is taken as a reference for designing the equivalent circuit. After designing the equivalent circuit to represent the coupling between antennas, the coupling coefficient between antennas can be extracted using Eq.(14). After obtaining the value and sign of k, the coupling matrix of the BSF, with the direct S/L coupling eliminated, can be derived using the inverse operation of CMS theory. However, the sign of the components of the coupling matrix will also vary due to the change in the sign of k. Eq.(15) is the same as Eq.(7) which is the coupling matrix when the sign of k is positive while Eq.(16) is the coupling matrix when the sign of k is negative.

$$\begin{pmatrix} 0 & -M_{S,1} & M_{S,2} & 0 \\ -M_{S,1} & -M_{1,1} & 0 & M_{L,1} \\ M_{S,2} & 0 & M_{2,2} & M_{L,2} \\ 0 & M_{L,1} & M_{L,2} & 0 \end{pmatrix} \quad (15)$$

$$\begin{pmatrix} 0 & M_{S,1} & -M_{S,2} & 0 \\ M_{S,1} & -M_{1,1} & 0 & M_{L,1} \\ -M_{S,2} & 0 & M_{2,2} & M_{L,2} \\ 0 & M_{L,1} & M_{L,2} & 0 \end{pmatrix} \quad (16)$$

After the derivation of coupling matrix, the equivalent circuit of BSF can be designed in ADS based on the derived coupling matrix. The equivalent circuits of each sign of k are illustrated in Fig.5(a) and Fig.5(b). Using these equivalent circuits, the proposed decoupling circuit can be realized for

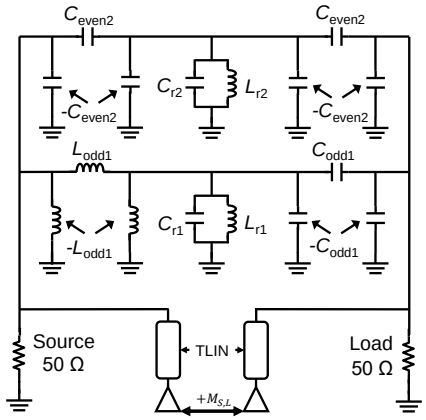

(a)

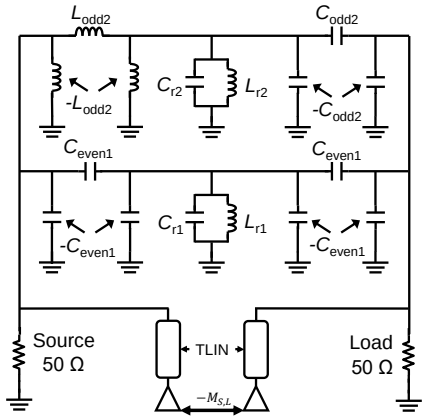

(b)

Fig. 5 Equivalent Circuit of Decoupling Circuit Utilizing Coupling Between Antennas. (a) Positive k. (b) Negative k

every sign of k formed from the coupling between antennas, utilizing the reference parameters mentioned in section 2.2.2.

3. Simulation and Experimental Results

In this section, the proposed decoupling circuit model is designed using ADS and HFSS software, following the procedures outlined in section 2.1. The design procedures for the proposed decoupling circuit are primarily divided into three subsections: the design of antennas and transmission lines, the design of the BSF eliminating direct S/L coupling, and the completion of the proposed decoupling circuit.

3.1 Design of Antenna and Transmission Line

A pair of monopole antennas operating at a center frequency of 840 MHz is designed by adjusting the antenna length. These monopole antennas are structured in a planar microstrip configuration using Megtron 7 from Panasonic as the dielectric substrate. The relative permittivity of dielectric substrate is 3.4 and the dielectric loss tangent is 0.001 while the dielectric substrate thickness is 0.75 mm and the copper strip thickness is 18 μm. With the information about the dielectric substrate and the aid of HFSS software, the monopole antenna length is fixed at 72.4 mm, while the distance between antennas is set at 24.9 mm ($0.12\lambda_0$).

After designing the monopole antennas, a pair of transmission microstrip lines is inserted at the end of the antennas to suppress the real part of the transmission admittance, $\mathrm{Re}[Y_{21}]$ by optimizing the length of the transmission microstrip line. As a result, the transmission length is fixed at 79 mm, providing sufficient suppression of $\mathrm{Re}[Y_{21}]$ as shown in Fig.6. The monopole antennas model shown in Fig.7 is fabricated and the comparisons are illustrated in Fig.8.

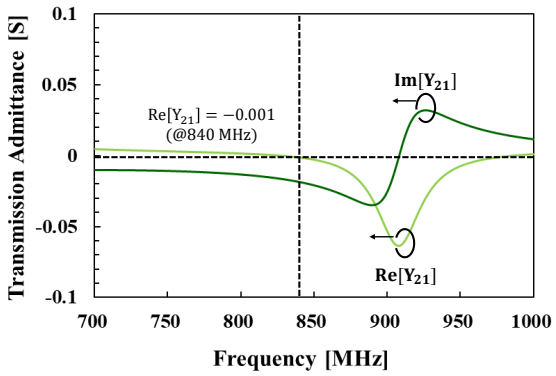

Fig. 6 Suppression of $\mathrm{Re}[Y_{21}]$ after Optimising Transmission Line Length.

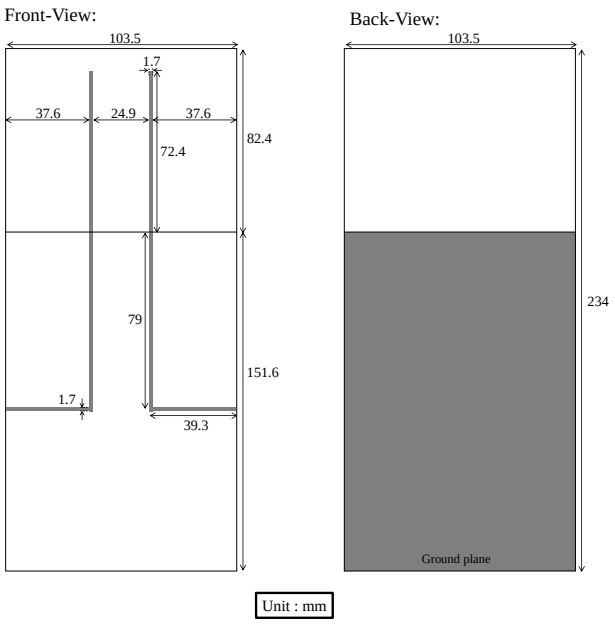

Fig. 7 Schematics of Monopole Antennas Pair.

The experimental results exhibit a good agreement with simulation results regarding return loss S_{11}, insertion loss

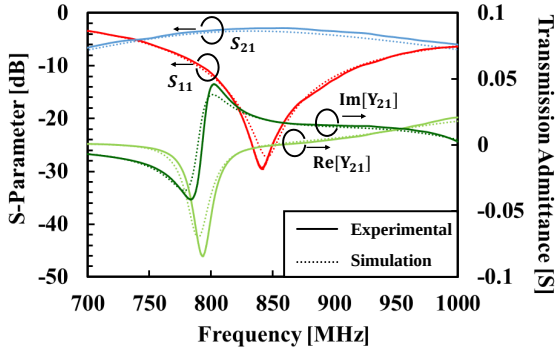

Fig. 8 Simulation and Experimental Results For Monopole Antennas Pair.

S_{21}, and transmission admittance Y_{21}. It's important to note that the waveform of the transmission admittance shown in Fig.8 differs from that in Fig.6 due to the insertion of horizontal feeding lines after the 79 mm optimized transmission lines from the antennas. Consequently, there is no deviation between experimental and simulation results, and the design correctness of the monopole antennas is verified.

3.2 Design of BSF Eliminating Direct S/L Coupling

Following the evaluation of the fabricated pair of monopole antennas, the coupling coefficient between antennas can be extracted based on the imaginary part of the transmission admittance Im[Y_{21}] in Fig.6. The equivalent circuit representing the coupling between antennas is designed with the aid of ADS software, using Im[Y_{21}] as a reference. An absolute value of 0.5824 is obtained using the equivalent circuit mentioned in section 2.2.3. Since the transmission admittance within the desired band is capacitive, k can be considered as -0.5824.

After obtaining the coupling coefficient between antennas, the filter characteristic parameters can be determined using the inverse operation of CMS theory, as shown in Table 1. The calculated coupling matrix eliminating the direct S/L coupling ($M_{S,L}$) based on filter characteristics parameters in Table 1 is shown in Eq.(17). Finally, the design indices can be extracted using Eqs.(3)-(6) as shown in Table 2.

Table 1 Band-Stop Filter Characteristics Parameters.

Characteristics Parameters	Value
Order of Chebyshev Response,N	2
Center Frequency,f_0	840 MHz
Bandwidth,BW	10 MHz
Insertion Loss,IL	30 dB
Reflection Zeros,RZs	[811 MHz , 868 MHz]

$$\begin{pmatrix} 0 & 1.1729 & -1.1236 & 0 \\ 1.1729 & -4.7315 & 0 & 1.1729 \\ -1.1236 & 0 & 4.5431 & 1.1236 \\ 0 & 1.1729 & 1.1236 & 0 \end{pmatrix} \quad (17)$$

Table 2 Design Indices of BSF.

Resonant Path	Resonant Frequency, f_i	External Q, $Q_{e,i}$
Even	863.01 MHz	34.1806
Odd	816.66 MHz	29.6819

Given that the sign of the coupling coefficient is negative, the equivalent circuit topology in Fig.5(b) is employed. The value of each element is determined with the assistance of ADS software based on the reference parameters mentioned in Eqs.(8)-(12). While observing the reference parameters, the determination of the element values is accomplished using the "Tuning" feature of ADS software. It's important to note that the BSF is designed separately without being connected to the antennas. This is because connecting the BSF to the antenna, the non-linear characteristics of the antenna make the reference parameters unobservable, and the design correctness of the BSF cannot be verified. During the BSF design process, the Q-factor of the chip elements is taken into account to minimize deviations between the fabricated model and the simulation model. The chip elements used in this paper are from Murata Manufacturing Company, Ltd. According to the Murata website, the Q-factor of the chip elements used is 50 for the inductor and 450 for the capacitor at 840 MHz. In the BSF design process, an issue of distortion in the transmission admittance occurred due to the low Q-factor of the chip elements used. The comparison of transmission admittance for different conditions of BSF is shown in Fig.9. Three conditions are considered for the comparison: ideal condition (infinite Q-factor), unmodified condition (low Q-factor chip elements), and a modified condition that will be discussed later.

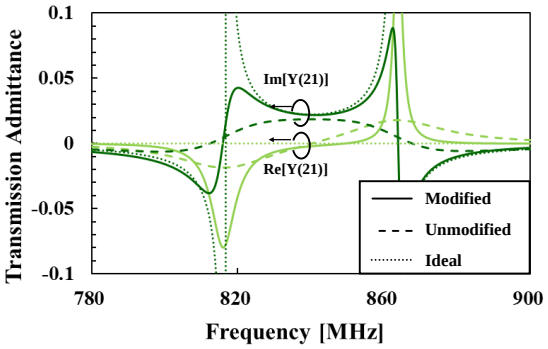

Fig. 9 Comparison of Transmission Admittance For Different Conditions of BSF.

In Fig.9, the distortion in transmission admittance is evident due to the low Q-factor of the chip elements. Under ideal design conditions for BSF, Re[Y_{21}] is almost considered as zero but a fluctuation in Re[Y_{21}] occurred due to the low Q-factor chip elements used in reality. This may degrade the decoupling effect of the BSF. The main reason for the distortion can be attributed to the low Q-factor shunt elements of the J-inverter used to represent the coupling between resonators and S/L. To suppress the distortion, the

shunt elements of the J-inverter must be removed. The shunt element of the J-inverter on the resonator's side can be removed due to its parallel arrangement with the resonators. The value of the resonator LC elements can be obtained by the simple equation of the parallel composition of impedance and admittance, as shown in Eqs.(18)-(20).

$$C_{r1}^{'} = C_{r1} - 2 * C_{even1} \tag{18}$$

$$C_{r2}^{'} = C_{r2} - C_{odd2} \tag{19}$$

$$L_{r2}^{'} = \frac{L_{r2} * -L_{odd2}}{L_{r2} - L_{odd2}} \tag{20}$$

Additionally, the shunt elements of the J-inverter on the S/L side is removed because its absence do not affect the stop-band characteristics. It is believed that this is absorbed by the parasitic component due to the long patterns of the transmission line used for mounting chip elements. Moreover, a quarter wavelength ($\lambda/4$) short-stub resonator is employed to reduce the number of low-Q-factor chip elements used [28]–[31]. Hence, the equivalent circuit of the proposed decoupling circuit is modified as shown in Fig.17. In this redesign process, only the even and odd mode resonators and the J-inverters are redesigned. While the modified result is shown in Fig.9 before.

Fig.9 demonstrates a significant improvement in both the real and imaginary parts of the transmission admittance by using a quarter-wavelength short-stub resonator and reducing the number of shunt elements in the equivalent circuit of the BSF. To further confirm the design correctness of the BSF equivalent circuit, the design indices of reflection phase and external Q for each resonant mode are verified. The verification results of external Q and reflection phase are given in Fig.11 respectively.

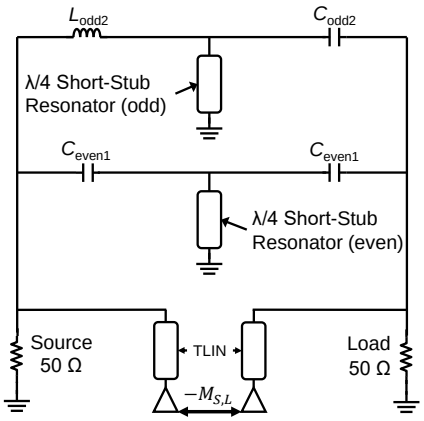

Fig. 10 Modified Equivalent Circuit of Proposed Decoupling Circuit.

In Fig.11, the designed BSF model exhibits a good agreement in both the external Q-factor and reflection phase for each resonant mode. Only below 6 % errors are observed between the simulation values and desired values mentioned in Table 2. Therefore, the designed BSF model can be regarded as a model with design correctness.

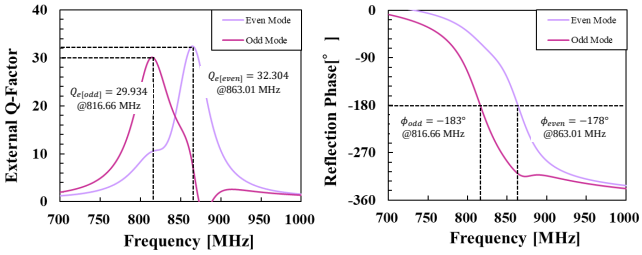

(a) (b)

Fig. 11 Simulation Results For Design Indices of BSF. (a) External Q-factor. (b) Reflection Phase.

Table 3 Element values and Dimension of Resonators of Decoupling Circuit.

Dimension & Element	Value[Simulation]	Value[Experimental]
Short-Stub Length (Even)	37.5 mm	37.5 mm
Short-Stub Width (Even)	4.5 mm	4.5 mm
$C_{even1[Equivalent]}$	0.82 pF	0.8 pF
Short-Stub Length (Odd)	48.6 mm	48.6 mm
Short-Stub Width (Odd)	6.8 mm	6.8 mm
$C_{odd2[Equivalent]}$	0.9 pF	1.11 pF
$L_{odd2[Equivalent]}$	34 nH	33 nH
L_{MC1}	5.6 nH	5.6 nH
C_{MC1S}	6.8 pF	6.8 pF
C_{MC1L}	2.4 pF	2.4 pF
L_{MC2}	3.9 nH	3.9 nH
C_{MC2S}	7.5 pF	7.5 pF
C_{MC2L}	0.8 pF	0.8 pF

3.3 Completion of Proposed Decoupling Circuit

The subsequent design step using HFSS software involves inserting the designed BSF in parallel between the pair of monopole antennas and utilizing the coupling between the antennas as the direct S/L coupling of the BSF to achieve stop-band characteristics within the desired bandwidth. Due to the insertion of the BSF, the impedance of the antennas becomes mismatched, necessitating the design of a matching circuit. To enhance the design flexibility of the matching circuit, this paper employs a π-shaped matching structure for the design.

The overall schematics of the proposed decoupling circuit are illustrated in Fig.12. The decoupling circuit model is fabricated and evaluated using Vector Network Analyzer (VNA). The evaluated results of the simulation model and the fabricated model, in terms of S-parameters and transmission admittance, are presented in Fig.13 respectively. The series element values and the dimensions of the resonator for both the simulation and fabricated models are listed in Table 4. Here, $C_{even1[Equivalent]}$, $C_{odd2[Equivalent]}$, and $L_{odd2[Equivalent]}$ represent the composite capacitances and inductance, respectively, while being the result of the series arrangement of chip elements to obtain precise element values.

The results in Fig.13 demonstrate that the fabricated

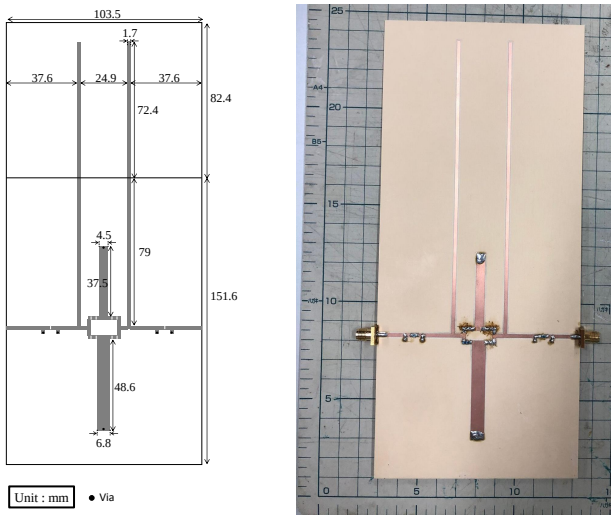

(a)

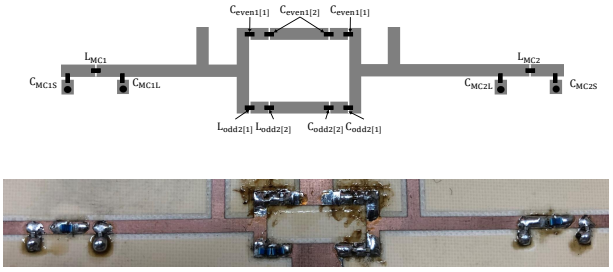

(b)

Fig. 12 Schematics of Proposed Decoupling Circuit. (a)Front View. (b) Enlarge View.

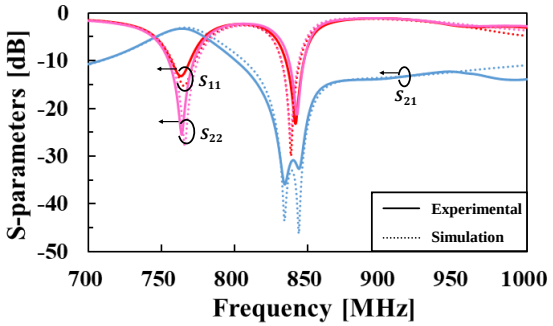

(a)

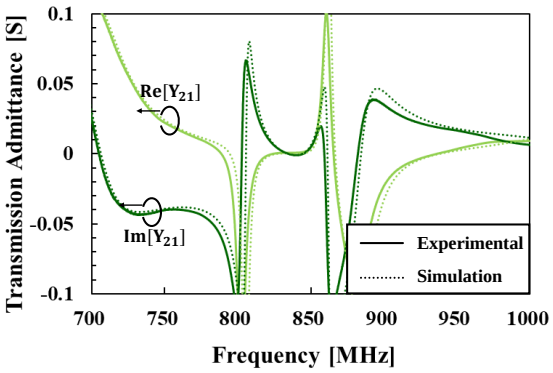

(b)

Fig. 13 Simulation and Experimental Results For Decoupling Circuit. (a) S-Parameters. (b) Transmission Admittance

model shows good agreement in both S-parameters and transmission admittance. However, there are some discrepancies in the dimensions of the resonator and the values of series elements between the simulation and fabrication models. These variations in values can be attributed to the manufacturing errors in the printed circuit board processing machine and the tolerance of chip element values used.

Subsequently, the fabricated model is compared with the desired specifications outlined in Table 1. As illustrated in Fig.13(a), an isolation level below -30 dB is achieved at the center frequency of 840 MHz with two attenuation poles, in accordance with the specified requirements for the BSF. This success is further supported by Fig.13(b), where both the real and imaginary parts of the transmission admittance between antennas are suppressed within the range ±0.001, as detailed in Section 2.1. However, the bandwidth of the decoupling circuit is increased by about 50 %, deviating from the desired value of 10 MHz. This deviation is attributed to the inherent challenge of fine-tuning the characteristics of the decoupling circuit due to the elimination of the direct S/L coupling of the BSF. Despite the bandwidth discrepancy, the decoupling circuit achieves the desired performance with 2 attenuation poles within the specified bandwidth, meeting the desired value of isolation. Furthermore, from Figure 13 (a), it is evident that both S11 and S22 ensure a reflection bandwidth of 13 MHz, indicating proper alignment. Here, the reflection bandwidth is defined with the operating frequency as the reference, where the reflection level is below -10 dB. At this point, an antenna with a reflection coefficient (S11 or S22 parameter) of -10 dB is considered proper because it indicates efficient transmission or absorption of 90% of the signal, with only 10% being reflected back towards the source. As the requirements set in Table 1 are fulfilled by all parameters– S11, S22, and S21– it can be concluded that the proposed method, which utilizes the coupling between antennas as direct S/L coupling, has been successful.

Lastly, the directivities of the antennas with and without the decoupling circuit are evaluated, as shown in Fig.14. From Fig.14, it can be seen that the antenna with the decoupling circuit exhibits improved radiation gain compared to the antenna without the decoupling circuit. The enhanced radiation gain can be attributed to the reduction in power loss at the load side by the decoupling circuit, thereby improving the radiation efficiency. The same phenomena can be observed through the radiation efficiency provided in Fig.15. The results in Fig.15 are measured the SG32 from the Microwave Vision Group. From Fig.15, it can be confirmed that the radiation efficiency is improved by adding the proposed circuit. While Fig.16 and 17 are provided as evidence supporting the aforementioned point, they illustrate the losses for the antenna without and with a decoupling circuit respectively, analyzed using an electromagnetic simulator, as

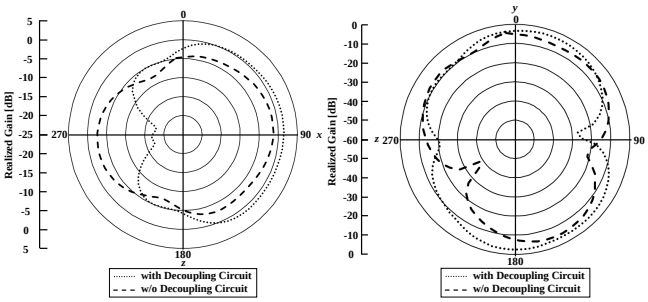

Fig. 14 Directivities of Antennas With and Without Decoupling Circuit. (a) H-plane. (b) E-plane.

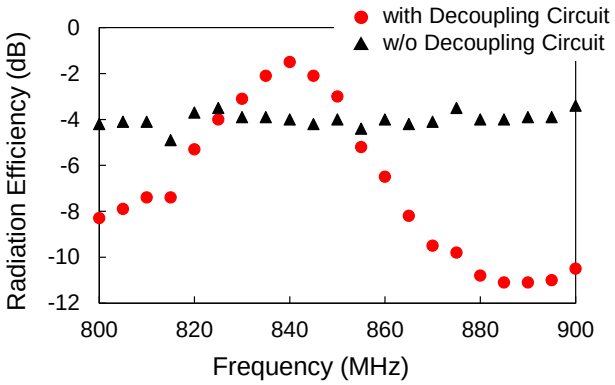

Fig. 15 Radiation Efficiency of Antennas with and without Decoupling Circuit.

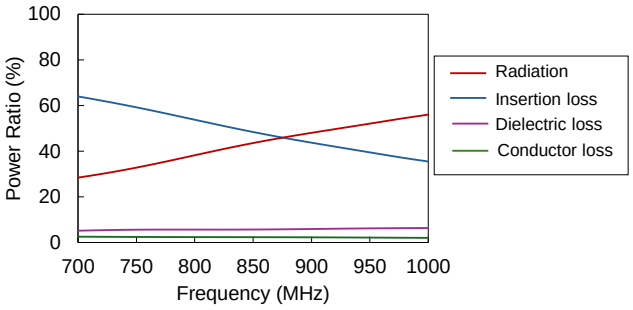

Fig. 16 Losses of Antennas without Decoupling Circuit.

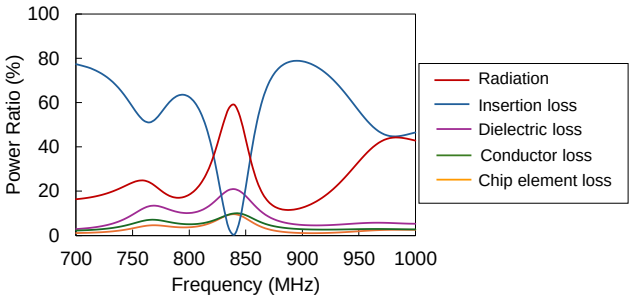

Fig. 17 Losses of Antennas without Decoupling Circuit.

direct measurement equipment for the losses is unavailable. In Fig.16, without the decoupling circuit, at the operating frequency of 840 MHz, the antenna radiated power is 42.5%, while the transmitted power between source and load sides is 49.4%. The losses comprise 5.9% dielectric loss and 2.3% conductor loss. Conversely, in Fig.17, with the decoupling circuit, at the same frequency, the antenna radiated power increases to 58.9%, with a significantly reduced transmitted power of 0.4%. However, the losses now include 21.0% dielectric loss, 9.9% conductor loss, and 9.6% chip component loss. These results indicate that the insertion lossof the decoupling circuit effectively suppresses transmitted power from 49.4% to 0.4% while enhancing radiated power from 42.5% to 58.9%. Therefore, by integrating the proposed circuit, there has been a notable enhancement in the efficiency of antennas.

4. Discussion

In this section, the novelty and superiority of the proposed method in comparison to conventional approaches will be expounded upon. A detailed comparison of the performance of the proposed method with previous works employing the decoupling method will be provided in Table 4. This comparison will encompass various dimensions including antenna spacing, coupling reduction, and bandwidth, thereby allowing for a comprehensive evaluation of the proposed method's efficacy and advantages over existing methodologies.

In terms of antenna spacing, it is noted that the proposed work demonstrates a larger antenna spacing when compared to other works. This difference stems from the deliberate choice of a low operating frequency for the antennas in the proposed work, resulting in a naturally larger antenna spacing. Additionally, the primary objective of this study is to validate the efficacy of the coupling matrix synthesis-based band-stop filter as a decoupling circuit. Consequently, the selection of a low operating frequency is deliberate, aiming to facilitate the design process of the decoupling circuit by ensuring ease of implementation. In future work, the verification of this proposed method will be conducted at higher operating frequencies, such as the Wi-Fi application band (2.45 GHz).

In terms of coupling reduction at the operating frequency, it is observed that the proposed work has offered a superior reduction in the coupling level compared to other works. Additionally, it should be noted that the 30 dB of coupling reduction achieved in this proposed work does not represent the limit of the achievable coupling reduction value. It is possible to achieve more than a 30 dB reduction by increasing the step of the band-stop filter, thereby enhancing the degree of freedom in the design of the band-stop filter. While the decoupling bandwidth of this proposed work is perceived as relatively narrow compared to other works, this limitation can be addressed through the adjustment of the band-stop filter's step size. By increasing the step of the band-stop

Table 4 Comparison of The Performance of The Proposed Work with Previous Works

Ref.	Decoupling Method	Antenna Spacing	Coupling Reduction	Bandwidth
[32]	Parallel-line-based coupling elements	$0.30\lambda_0$@ 2.0 GHz	26.2dB	N/A
[33]	Coupled Resonator	$0.077\lambda_0$@2.45 GHz	15dB	4%
[34]	T-stub	$0.081\lambda_0$@2.45 GHz	13dB	6.1%
[35]	Wilkinson power divider (dual band)	$0.045\lambda_0$@1.0 GHz	33dB	N/A
[36]	Band-pass filter	$0.036\lambda_0$@2.45 GHz	>20dB	N/A
[37]	Reactive Element DMN	$0.08\lambda_0$@2.4 GHz	>20dB	N/A
[38]	Two-layer Decoupling	$0.108\lambda_0$@2.1 GHz	>20dB	N/A
[39]	Even-odd-mode DMN	$0.259\lambda_0$@2.615 GHz	15dB	38.60%
[40]	Two-layer DMN	$0.310\lambda_0$@3.5 GHz	17dB	15.70%
[41]	Resistive DMN	$0.069\lambda_0$@2.45 GHz	22dB	4%
This Work	Coupling Matrix Synthesis	$0.07\lambda_0$@840 MHz	>30dB	1.7%

filter, it becomes possible to expand the bandwidth, thereby improving the efficacy of the decoupling mechanism. This approach offers a means to mitigate the perceived drawback and enhance the overall performance of the proposed method in decoupling applications.

Next, the comparison in terms of the size of the decoupling circuit will be addressed. It is noted that the proposed work exhibits a larger decoupling circuit structure compared to other works. This discrepancy primarily arises from the intentional selection of a low operating frequency. However, it is worth noting that this limitation can potentially be addressed by elevating the operating frequency, leveraging the phenomenon of wavelength shortening at higher frequencies. Moreover, an alternative avenue for addressing this issue involves miniaturizing the decoupling circuit in the proposed work. This could be achieved by integrating all of its constituent elements through the Low Temperature Co-fired Ceramics (LTCC) method, a technique known for its capability to enable compact and efficient circuit designs.

Last but not least, attention will be directed towards discussing the prospects of the proposed method. While the current study focuses solely on the application of the proposed method to a 1 x 1 antennas array, corresponding to the In-Band Full-Duplex communication method, its potential extends further. The method could be effectively extended to MIMO communication methods, given the similar interference issues encountered in such systems. These issues primarily stem from the coupling between antenna arrays due to their closely packed or asymmetric arrangement . By leveraging Coupling Matrix Synthesis-based filter theory to cancel or suppress this coupling, the proposed method could be successfully applied to MIMO systems as well, scaling up from a 1 x 1 to a 2 x 2 antennas array and beyond. As part of future work, the proposed method will be validated within the context of a 2 x 2 antennas array configuration. Furthermore, the implementation of the LTCC method to miniaturize the decoupling structure holds promise for reducing the overall size of the MIMO communication module compared to current market offerings. This advancement carries potential benefits in terms of portability, cost-effectiveness, and performance enhancement in communication systems.

5. Conclusion

This paper proposed the design procedures for a decoupling circuit utilizing the coupling between antennas. A decoupling circuit is designed, featuring two quarter-wavelength short-stub resonators and utilizing coupling between antennas as direct S/L coupling of BSF. Subsequently, the designed circuit is fabricated and evaluated. The fabricated model exhibits good decoupling characteristics, achieving a 30 dB isolation level within a 15 MHz bandwidth while operating at the center frequency of 840 MHz. Furthermore, the confirmation of an improvement in radiation gain has been established.

Acknowledgments

The authors would like to thank Yuichi Miyaji for the lively discussion. This work is supported by the VLSI Design and Education Center (VDEC) and the University of Tokyo in collaboration with Keysight Technologies, Ltd.

References

[1] K. Shafique, B. A. Khawaja, F. Sabir, S. Qazi and M. Mustaqim, "Internet of Things (IoT) for Next-Generation Smart Systems: A Review of Current Challenges, Future Trends and Prospects for Emerging 5G-IoT Scenarios," in *IEEE Access*, vol. 8, pp. 23022-23040, 2020, doi: 10.1109/ACCESS.2020.2970118.

[2] M. Alsabah et al., "6G Wireless Communications Networks: A Comprehensive Survey," in *IEEE Access*, vol. 9, pp. 148191-148243, 2021, doi: 10.1109/ACCESS.2021.3124812.

[3] X. Chen, S. Zhang and Q. Li, "A Review of Mutual Coupling in MIMO Systems," in "IEEE Access", vol. 6, pp. 24706-24719, 2018, doi: 10.1109/ACCESS.2018.2830653.

[4] M. A. Jensen, and J. W. Wallace, "A review of antennas and propagation for MIMO wireless communications, "*IEEE Trans. Antennas Propag.*, vol.52, no.11, pp.2810–2824, 2004. DOI: 10.1109/TAP.2004.835272.

[5] A. Sabharwal, P. Schniter, D. Guo, D. W. Bliss, S. Rangarajan and R. Wichman, "In-Band Full-Duplex Wireless: Challenges and Opportunities," in *IEEE Journal on Selected Areas in Communications*, vol. 32, no. 9, pp. 1637-1652, Sept. 2014, doi: 10.1109/JSAC.2014.2330193.

[6] M. Katanbaf, K. D. Chu, T. Zhang, C. Su, and J. C. Rudell, "Two-WayTraffic Ahead, "*IEEE Microw. Mag.*, vol.20, No.2, pp.25–35, 2019. DOI: 10.1109/MMM.2018.2880489.

[7] D. Dhara, G. Gupta, T. Zhang, and A. R. Harish, "A Wideband Polarization Diversity 3D MIMO Antenna, "*2018 IEEE Indian Conference on Antennas and Propogation (InCAP)*, Hyderabad, India, pp.1–4, Dec. 2018. DOI: 10.1109/INCAP.2018.8770770.

[8] Q. Hua, Y. Huang, A. Alieldin, C. Song, T. Jia, and X. Zhu, "A Dual-Band Dual-Polarized Base Station Antenna Using a Novel Feeding Structure for 5G Communications,"*IEEE Access*, vol.8, pp.63710–63717, 2020. DOI: 10.1109/ACCESS.2020.2984199.

[9] K. Tong, H. Tang, A. Al-Armaghany, and W. Hong, "Low-Profile Orthogonally Tripolarized Antennas,"*IEEE Antennas Wirel. Propag. Lett.*, vol.12, pp.876–879, 2013, DOI: 10.1109/LAWP.2013.2271971.

[10] J. Zhu, S. Li, S. Liao, and Q. Xue, "Wideband Low-Profile Highly Isolated MIMO Antenna With Artificial Magnetic Conductor," in *IEEE Antennas Wirel. Propag. Lett.*, vol.17, no.3, pp.458–462, 2018. DOI: 10.1109/LAWP.2018.2795018.

[11] M. Amjadi and K. Sarabandi, "Ultra-Wideband, Compact, and High-Gain Two-Port Antenna System for Full-Duplex Applications," in

IEEE Transactions on Antennas and Propagation, vol. 69, no. 11, pp. 7173-7182, Nov. 2021, doi: 10.1109/TAP.2021.3076266.

[12] Z. Wang, Y. Ning and Y. Dong, "Hybrid Metamaterial-TL-Based, Low-Profile, Dual-Polarized Omnidirectional Antenna for 5G Indoor Application," in *IEEE Transactions on Antennas and Propagation*, vol. 70, no. 4, pp. 2561-2570, April 2022, doi: 10.1109/TAP.2021.3137242.

[13] M. A. Sufian, N. Hussain, H. Askari, S. G. Park, K. S. Shin and N. Kim, "Isolation Enhancement of a Metasurface-Based MIMO Antenna Using Slots and Shorting Pins," in *IEEE Access*, vol. 9, pp. 73533-73543, 2021, doi: 10.1109/ACCESS.2021.3079965.

[14] J. Yin, Y. Jia, S. Yang and H. Zhai, "Design of a Composite Decoupling Structure for Dual-Band Dual-Polarized Base Station Array," in *IEEE Antennas and Wireless Propagation Letters*, vol. 21, no. 7, pp. 1408-1412, July 2022, doi: 10.1109/LAWP.2022.3170081.

[15] B. Liu, X. Chen, J. Tang, A. Zhang and A. A. Kishk, "Co- and Cross-Polarization Decoupling Structure With Polarization Rotation Property Between Linearly Polarized Dipole Antennas With Application to Decoupling of Circularly Polarized Antennas," in *IEEE Transactions on Antennas and Propagation*, vol. 70, no. 1, pp. 702-707, Jan. 2022, doi: 10.1109/TAP.2021.3097769.

[16] S. C. Chen, Y. S. Wang, and S. J. Chung, " A Decoupling Technique for Increasing the Port Isolation Between Two Strongly Coupled Antennas, "*IEEE Trans. Antennas Propag.*, vol.56, no.12, pp.3650–3658, 2008. DOI: 10.1109/TAP.2008.2005469.

[17] Cheng-Hsu Wu, Chia-Lin Chiu, and Tzyh-Ghuang Ma, " Very Compact Fully Lumped Decoupling Network for a Coupled Two-Element Array, "*IEEE Antennas Wirel. Propag. Lett.*, vol.15, pp.158–161, 2015. DOI: 10.1109/LAWP.2015.2435793.

[18] K. Qian, G. Huang, J. Liang, B. Qian, and T. Yuan, "An LTCC Interference Cancellation Device for Closely Spaced Antennas Decoupling,"*IEEE Access*, vol.6, pp.68255–68262, 2018. DOI: 10.1109/ACCESS.2018.2879569.

[19] K. Qian, " A Compact LTCC Decoupling-Network Based on Coupled-Resonator for Antenna Interference Suppression of Adjacent Frequency Bands,"*IEEE Access*, vol.7, pp.25485–25492, 2019. DOI: 10.1109/ACCESS.2019.2900248.

[20] L. Zhao, F. Liu, X. Shen, G. Jing, Y. Cai, and Y. Li, "A High-Pass Antenna Interference Cancellation Chip for Mutual Coupling Reduction of Antennas in Contiguous Frequency Bands," *IEEE Access*, vol.6, pp.38097–38105, 2018. DOI: 10.1109/ACCESS.2018.2853709.

[21] K. Nishimoto, H. Makimura, T. Yanagi, Y. Nishioka, N. Yoneda and, H. Miyashita, "Narrowband/wideband decoupling networks for antenna arrays and excitation ditribution control," *2018 International Workshop on Antenna Technology (iWAT)*, Jun. 2018. pp.1–4, DOI: 10.1109/IWAT.2018.8379122.

[22] R. J. Cameron, " General Coupling Matrix Synthesis Methods for Chebyshev Filtering Functions, "*IEEE Trans. Microw. Theory Techn.*, vol.47, no.4, pp.433–442, 1999. DOI: 10.1109/22.754877.

[23] R. J. Cameron," Advanced coupling matrix synthesis techniques for microwave filters, "*IEEE Trans. Microw. Theory Techn.*, vol.51, no.1, pp.1–10, 2003. DOI: 10.1109/TMTT.2002.806937.

[24] R. J. Cameron, and M. Yu, Y. Wang, " Direct-Coupled Microwave Filters With Single and Dual Stopbands, "*IEEE Trans. Microw. Theory Techn.*, vol.53, no.11, pp.3288–3296, Nov. 2005. DOI: 10.1109/TMTT.2005.859032.

[25] S. Amari, and U. Rosenberg, " Direct Synthesis of a New Class of Bandstop Filters, "*IEEE Trans. Microw. Theory Techn.*, vol.52, no.2, pp.607–616, Feb. 2004. DOI: 10.1109/TMTT.2003.821939.

[26] M. Ohira, K. Toshiki, and M. Zhewang, " A Fully Canonical Bandpass Filter Design Using Microstrip Transversal Resonator Array Configuration, "*IEICE Trans. on Electron.*, vol.E99-C, no.10, pp.1122–1129, Oct. 2016. DOI: 10.1587/transele.E99.C.1122.

[27] M. Ohira, and M. Zhewang, " A Parameter-Extraction Method for Microwave Transversal Resonator Array Bandpass Filters With Direct Source/Load Coupling, "*IEEE Trans. Microw. Theory Techn.*, vol.61, no.5, pp.1801–1811, 2013. DOI: 10.1109/TMTT.2013.2252187.

[28] J. -X. Xu, X. Y. Zhang and Y. Yang, "High-Q-Factor Dual-Band Bandpass Filter and Filtering Switch Using Stub-Loaded Coaxial Resonators," *2019 IEEE MTT-S International Wireless Symposium (IWS)*, Guangzhou, China, 2019, pp. 1-3, doi: 10.1109/IEEE-IWS.2019.8803878.

[29] D. Y. Jung, K. C. Eun and C. S. Park, "High-Q Circular LTCC Resonator Using Zigzagged Via Posts and a $\lambda/4$ Short Stub for Millimeter-Wave System-on-Package Applications," in *IEEE Transactions on Advanced Packaging*, vol. 32, no. 1, pp. 216-222, Feb. 2009, doi: 10.1109/TADVP.2008.2007237.

[30] Pozar, D. M., Microwave Engineering (4th ed.), Hoboken, NJ: Wiley, 2011.

[31] Hong, J.-S., & Lancaster, M. J., Microstrip Filters for RF/Microwave Applications., Hoboken, NJ: Wiley, 2011.

[32] K. -D. Xu, H. Luyen and N. Behdad, "A Decoupling and Matching Network Design for Single- and Dual-Band Two-Element Antenna Arrays," in IEEE Transactions on Microwave Theory and Techniques, vol. 68, no. 9, pp. 3986-3999, Sept. 2020, doi: 10.1109/TMTT.2020.2989120.

[33] L. Zhao and K. -L. Wu, "A Dual-Band Coupled Resonator Decoupling Network for Two Coupled Antennas," in IEEE Transactions on Antennas and Propagation, vol. 63, no. 7, pp. 2843-2850, July 2015.

[34] J. Sui and K. -L. Wu, "A General T-Stub Circuit for Decoupling of Two Dual-Band Antennas," in IEEE Transactions on Microwave Theory and Techniques, vol. 65, no. 6, pp. 2111-2121, June 2017.

[35] M. Li, J. M. Yasir, K. L. Yeung and L. Jiang, "A Novel Dual-Band Decoupling Technique," in IEEE Transactions on Antennas and Propagation, vol. 68, no. 10, pp. 6923-6934, Oct. 2020.

[36] M. M. Albannay, J. C. Coetzee, X. Tang and K. Mouthaan, "Dual-Frequency Decoupling for Two Distinct Antennas," in IEEE Antennas and Wireless Propagation Letters, vol. 11, pp. 1315-1318, 2012.

[37] K. -C. Lin, C. -H. Wu, C. -H. Lai and T. -G. Ma, "Novel Dual-Band Decoupling Network for Two-Element Closely Spaced Array Using Synthesized Microstrip Lines," in IEEE Transactions on Antennas and Propagation, vol. 60, no. 11, pp. 5118-5128, Nov. 2012.

[38] Y. -F. Cheng and K. -K. M. Cheng, "A Novel Dual-Band Decoupling and Matching Technique for Asymmetric Antenna Arrays," in IEEE Transactions on Microwave Theory and Techniques, vol. 66, no. 5, pp. 2080-2089, May 2018.

[39] Y. -F. Cheng, D. Li, S. Chen and G. Wang, "A Novel Wideband Decoupling Method Based on Even-Odd-Mode Analysis and Genetic Algorithm Optimization," in IEEE Antennas and Wireless Propagation Letters, vol. 22, no. 10, pp. 2507-2511, Oct. 2023.

[40] Y. -F. Cheng and K. -K. M. Cheng, "Compact Wideband Decoupling and Matching Network Design for Dual-Antenna Array," in IEEE Antennas and Wireless Propagation Letters, vol. 19, no. 5, pp. 791-795, May 2020.

[41] S. N. Venkatasubramanian, L. Li, A. Lehtovuori, C. Icheln and K. Haneda, "Impact of Using Resistive Elements for Wideband Isolation Improvement," in IEEE Transactions on Antennas and Propagation, vol. 65, no. 1, pp. 52-62, Jan. 2017.

Zhi Earn TAN received the B.E. degree in electrical and electronic information engineering from the Toyohashi University of Technology, Toyohashi, Japan, in 2022, where he is currently pursuing the master's degree. He is currently with the Toyohashi University of Technology, where he is engaged in the development of decoupling network for mutual coupling between antennas.

Kenjiro MATSUMOTO received the B.E. degree in electrical and electronic information engineering from the Toyohashi University of Technology, Toyohashi, Japan, in 2023, where he is currently pursuing the master ' s degree. He is currently with the Toyohashi University of Technology, where he is engaged in the development of Decoupling network for mutual coupling between antennas.

Masaya TAKAGI received the B.E. and M.E. degree in electrical and electronic information engineering from the Toyohashi University of Technology, Toyohashi, Japan, in 2019 and 2021, respectively. He was engaged in the development of decoupling network for mutual coupling between antennas in his B.E. and M.E. degree.

Hiromasa SAEKI received a B.E. and M.E. degree in condensed matter physics from Osaka University, Osaka, Japan, in 2000 and 2002 , respectively. From 2001 to 2003, he worked as a research fellow of the Japan Society for the Promotion of Science. From 2004 to 2006, he was a research assistant of Osaka University. In December 2006, he joined Murata Manufacturing Co. Ltd., where he was involved in the development of SAW filters, light emitting diodes, thin film capacitors and wireless power transfers.

Masaya TAMURA received the B.E. and M.E. degrees from Okayama University, Okayama, Japan in 2001 and 2003, respectively, and the Ph.D. degree from Kyoto University, Kyoto, Japan in 2012. From April 2003 to March 2014, he has worked at Panasonic Corporation, where he has been engaged in research and development on high-frequency components including light-wave, especially microwave filters, metamaterials, and plasmonics. In April 2014, he joined the Toyohashi University of Technology, where he is currently a Professor of Electrical and Electronic Information Engineering. His current research interests include microwave circuits and wireless power transfer. Dr. Tamura was the recipient of the IEEE MTT-S Outstanding Young Engineer Award in 2015. He has also received the 2012 IEEE MTT-S Japan Young Engineer Award and the 2012 Michiyuki Uenohara Memorial Award.